Geophysical Research Letters

RESEARCH LETTER
10.1029/2025GL114615

# Physical Properties Controlling Earthquake Ruptures: Two Study Cases Along the South American Subduction Zone

**Sergio Leon-Rios[1], Andreas Rietbrock[2], Lidong Bie[3], Susan Beck[4], Philippe Charvis[5], Diana Comte[1,6], Audrey Galve[5], Anne Meltzer[7], Steven Roecker[8], Mario Ruiz[9], and Monica Segovia[9]**

[1]Advanced Mining Technology Center (AMTC), Facultad de Ciencias Físicas y Matemáticas, Universidad de Chile, Santiago, Chile, [2]Geophysical Institute, Karlsruhe Institute of Technology, Karlsruhe, Germany, [3]School of Environmental Sciences, University of East Anglia, Norwich, UK, [4]Department of Geosciences, University of Arizona, Tucson, AR, USA, [5]Université Côte d'Azur, IRD, CNRS, Observatoire de la Côte d'Azur, Valbonne, France, [6]Departamento de Geofísica, Facultad de Ciencias Físicas y Matemáticas, Universidad de Chile, Santiago, Chile, [7]Department of Earth & Environmental Sciences, Lehigh University, Bethlehem, PA, USA, [8]Environmental Sciences, Rensselaer Polytechnic Institute, Troy, NY, USA, [9]Escuela Politécnica Nacional, Instituto Geofísico, Quito, Ecuador

**Abstract** Seismic velocity models were compared with coseismic slip distributions for two megathrust earthquakes that occurred along the South American subduction zone. By analyzing the distribution of Vp/Vs ratios, we found that seismic anomalies with values higher or lower than the average coincide with the boundaries of the earthquake ruptures. In contrast, the regions characterized by intermediate Vp/Vs values may represent a mechanical "sweet spot" where the physical properties create favorable conditions for sustained rupture propagation. Our methodology, which combines the Vp/Vs distribution and the analysis of coseismic slip models, could reveal the rupture-prone regions and the likely magnitude of potential earthquakes, providing relevant information for seismic hazard assessment.

**Plain Language Summary** We compared models of seismic velocity ratio (compressional velocity/shear velocity) with slip distributions from two megathrust earthquakes along the South American subduction zone. Our analysis shows that regions with seismic anomalies of higher or lower than average values tend to coincide with the edges of earthquake ruptures. In contrast, regions with intermediate values seem to allow ruptures to propagate over longer distances. This suggests that these areas have physical properties that support sustained rupture. Therefore, our approach helps to identify regions prone to large earthquake ruptures and to estimate their potential size, providing useful insights for seismic hazard assessment.

**Key Points:**

- We compared seismic velocity models with the coseismic slip from two megathrust earthquakes along the South American subduction zone
- Seismic anomalies distributed along the slab interface play a critical role in controlling the extent of earthquake rupture
- Earthquakes need to occur in a "sweet spot" of physical properties for the rupture to propagate greater distances

**Supporting Information:**

Supporting Information may be found in the online version of this article.

**Correspondence to:**

A. Rietbrock,
andreas.rietbrock@kit.edu

**Citation:**

Leon-Rios, S., Rietbrock, A., Bie, L., Beck, S., Charvis, P., Comte, D., et al. (2025). Physical properties controlling earthquake ruptures: Two study cases along the South American subduction zone. *Geophysical Research Letters*, *52*, e2025GL114615. https://doi.org/10.1029/2025GL114615

Received 2 JAN 2025
Accepted 11 JUL 2025

**Author Contributions:**

**Conceptualization:** Andreas Rietbrock, Lidong Bie, Audrey Galve
**Data curation:** Sergio Leon-Rios, Andreas Rietbrock
**Formal analysis:** Sergio Leon-Rios, Lidong Bie
**Funding acquisition:** Andreas Rietbrock, Susan Beck, Philippe Charvis, Audrey Galve, Anne Meltzer, Steven Roecker
**Investigation:** Sergio Leon-Rios, Andreas Rietbrock
**Methodology:** Sergio Leon-Rios, Andreas Rietbrock, Lidong Bie
**Project administration:** Andreas Rietbrock, Susan Beck, Philippe Charvis, Audrey Galve,



## 1. Introduction

Megathrust earthquakes in subduction zones are among the most destructive geological events on our planet. During the last decades, studies along the plate interface have discussed their limits identifying three main regions: (a) the aseismic updip portion mostly consisting of unconsolidated sediments and stable sliding clays (Byrne et al., 1988; Vrolijk, 1990); (b) the seismogenic zone, where thrust earthquakes occur; and (c) the aseismic downdip portion with stable slip that is thermally confined (Hyndman & Wang, 1993; Tichelaar & Ruff, 1993) or controlled by the interaction of the megathrust with the forearc Moho (Ruff & Tichelaar, 1996). Along the seismogenic zone, the earthquake rupture area is a topic with many uncertainties and questions that remain open. One of these is which physical properties control the size and limits of earthquakes? In that line, large megathrust earthquakes of recent decades have provided opportunities to find answers. At first order, the rupture limits of earthquakes have often been associated with local features such as ridges and peninsulas (Bilek, 2010; Bilek et al., 2003; Collot et al., 2017; Wang & Bilek, 2011; Watts et al., 2010). When studied locally, these structures show similar characteristics using different methods, with low b-values (e.g., Sobiesiak et al., 2007; Wiemer & Katsumata, 1999), low Poisson ratios (e.g., Di Stefano et al., 2011), and low Vp/Vs (Pasten-Araya et al., 2018) for the case of Mejillones Peninsula in northern Chile. However, challenges in studying the oceanic-continental margin, such as the limited instrumentation and coarse resolution of offshore seismic models, as well as the inherent difficulty of directly observing physical properties along the slab (e.g., temperature, density, velocity), have prevented correlating the characteristics of the Earth's interior and the extent of megathrust earthquakes. There are few studies for New Zealand (Reyners & Eberhart-Phillips, 2009) and for Japan (e.g., Mishra et al., 2003) linking seismic velocity anomalies to earthquake rupture but only few efforts have been made for the

Anne Meltzer, Steven Roecker, Mario Ruiz, Monica Segovia
**Resources:** Mario Ruiz, Monica Segovia
**Software:** Sergio Leon-Rios
**Supervision:** Andreas Rietbrock, Diana Comte
**Validation:** Sergio Leon-Rios
**Visualization:** Lidong Bie
**Writing – original draft:** Sergio Leon-Rios
**Writing – review & editing:** Andreas Rietbrock, Lidong Bie, Susan Beck, Philippe Charvis, Diana Comte, Audrey Galve, Anne Meltzer, Steven Roecker, Mario Ruiz, Monica Segovia

South American subduction zone due to limited seismic data availability. Latest studies using precise earthquake relocations in the Ecuadorian margin have shown the complexity within the slab interface and the importance of conceptualizing the megathrust as a fault network, rather than viewing it as a single plane (Chalumeau et al., 2024).

A direct method to further investigate the seismic properties along the slab interface is tomographic images from travel-time arrivals, which allow us to obtain the variation of P- and S-wave velocities (Vp and Vs) and their corresponding ratios (Vp/Vs) in certain regions of interest. The Vp/Vs ratio can be used as a good indicator to analyze the behavior of the seismogenic zone during the different stages of the seismic cycle. Low Vp/Vs values are generally associated with consolidated rocks, indicating low porosity, a lower degree of hydration and also low fluid pressure. In contrast, high Vp/Vs values can be associated with less consolidated or fluid-filled areas where increased porosity, higher degrees of hydration and higher fluid pressure contribute to the seismic velocity contrast. Variations in Vp/Vs also depend on lithology; for example, quartz-rich rocks tend to have lower Vp/Vs ratios, while clay-rich and serpentinized materials have higher values, reflecting their increased water content and altered mineralogy. Additionally, high Vp/Vs ratios have been related to anisotropy, which therefore may be particularly relevant for particular minerals (Miller et al., 2021).

Thus, by comparing the distribution of Vp/Vs values with other seismological and geodetic observations, such as locking and coseismic slip, it is possible to better understand the physical properties of areas affected by large earthquakes.

By using aftershocks recorded shortly after the mainshock, Vp/Vs models have highlighted seismic anomalies that collocate with the boundaries of the rupture extent. For the 2012 Mw 7.6 Nicoya, Costa Rica earthquake, Audet and Schwartz (2013) observed high Vp/Vs ratios in regions that correlated with the southeastern end of the rupture. Similar results were found for the 2015 Illapel earthquake (Mw 8.3) in Chile, where the southern edge of the rupture stopped in an area of high Vp/Vs (Liu et al., 2018). Husen and Kissling (2001) described changes in the Vp/Vs distribution following the 1995 Mw 8.0 Antofagasta, Chile earthquake. Here, they described the time-dependent evolution of the Vp/Vs ratios caused by a large earthquake and the implications for the unfolding aftershock sequence.

For the interseismic period, the Vp/Vs derived from the background seismicity contribute to imaging the seismic anomalies and exploring the implications for megathrust earthquake development and rupture extent (Haberland et al., 2009).

This work considers two cases along the South American margin where seismic velocity models of the slab interface are available for different stages of the seismic cycle. First, we study the postseismic phase and compare the distribution of seismic velocity anomalies (Leon-Rios et al., 2021) with the coseismic slip of the 2016 Mw 7.8 Pedernales, Ecuador earthquake. In addition, by combining a grid search approach and rupture-scaling parameters, we devised a novel technique to further explore the possible rupture scenarios in the area. In the second, we study the interseismic period with a Vp/Vs model (Leon-Rios et al., 2024) derived ~30 years after the 1995 Mw 8.0 Antofagasta earthquake.

The analysis of the distribution of Vp/Vs anomalies along the subduction interface, together with published coseismic slip models, can help to characterize the physical properties of the South American megathrust. While this approach does not directly estimate the magnitude of future earthquakes, and can be limited by the variability of imaging resolution, it can contribute to a broader understanding of the factors that may influence the rupture behavior along the South American margin and provide complementary information for seismic hazard assessment.

## 2. The 2016 Pedernales, Ecuador Earthquake

On 16 April 2016, the central part of the Ecuadorian margin was affected by a Mw 7.8 megathrust earthquake that ruptured an area of ~100 × 50 km$^2$ (Figure 1). The mainshock activated a large national and international rapid response that, within a few days after the earthquake, installed a dense temporary and amphibious seismic network of 65 seismometers that recorded the aftershock sequence for one year (Meltzer et al., 2019; Regnier et al., 2016). The backbone seismic and geodetic observations constrained the rupture slip, while the seismic emergency deployment captured the unfolding aftershocks (Agurto-Detzel et al., 2019; Leon-Rios et al., 2019, 2021; Soto-Cordero et al., 2020). Furthermore, Vaca et al. (2018) discussed the correlation between the northern

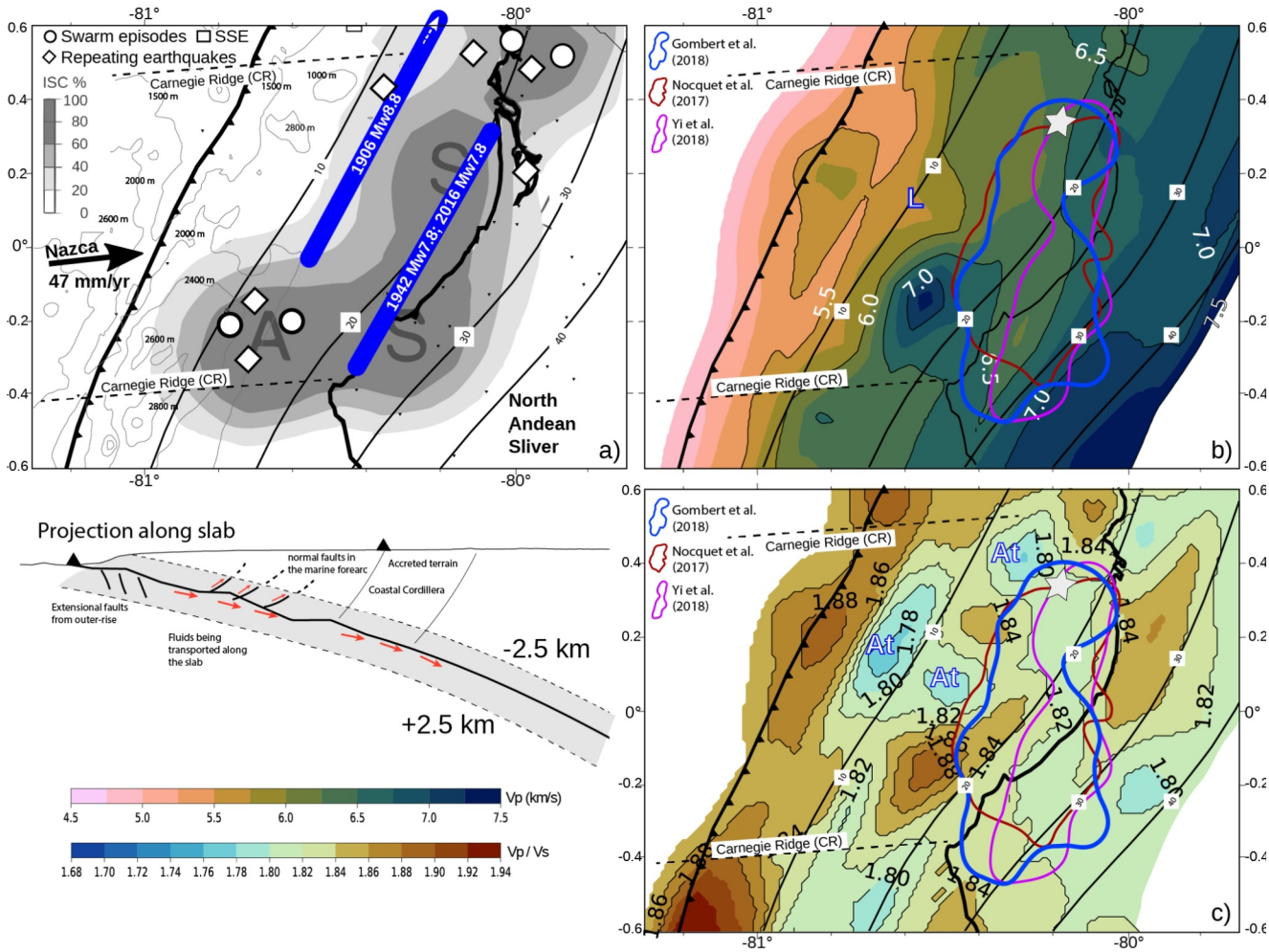


**Figure 1.** (a) Seismotectonic of Ecuador margin. Blue lines show the 1906 Mw 8.8, 1942 Mw 7.8 earthquakes. Circles, diamonds, and squares indicate swarms, repeating earthquakes, and SSE, respectively. Interseismic coupling by Nocquet et al. (2014) and offshore residual bathymetry (Agurto-Detzel et al., 2019) are shown in background contours. (a) Aseismic zone, S: seismic zone. (b–c) Vp and Vp/Vs models projected along the slab interface (see inset cross section). Star represents the epicenter of the 2016 Mw 7.8 Pedernales earthquake. The colored contours show the 2 m coseismic slip by Gombert et al. (2018) in blue, Nocquet et al. (2017) in red, and Yi et al. (2018) in purple. The inset cross section represents the projected region along a ±2.5 km region around the slab interface. The main factors controlling the differences in seismic velocities are highlighted.

limit of the 2016 rupture and the occurrence of slow slip events. Similarly, observations of recurrent earthquakes and seismic swarms before (e.g., Rolandone et al., 2018; Segovia, 2009; Segovia et al., 2018; Vaca et al., 2009) and after (Chalumeau et al., 2021) the earthquake provide additional support for the hypothesis that slow slip and seismic precursors may play a role in defining the rupture limits of large earthquakes.

The Pedernales earthquake also triggered further investigations with dense seismic networks and offshore experiments (e.g., HIPER, HIPER 2.0; Galve, 2020; Galve et al., 2021), which revealed meters-thick active faults in the subduction interface (Chalumeau et al., 2024). To further explore what physical properties might have controlled the rupture extent of the Pedernales earthquake, we combined the seismic imaging and the constraints for the coseismic slip distribution.

## 3. Seismic Velocity Model and Coseismic Slip for the 2016 Pedernales, Ecuador Earthquake

To further investigate the relationship between seismic anomalies and earthquake rupture extent, we explored the Vp and Vp/Vs distribution along the plate interface. To account for model resolution, we averaged the values over a plate with ±2.5 km (Figure 1, Yamamoto et al., 2014). We used an updated plate boundary generated by

combining the trench location derived by (Collot et al., 2005), the relocated seismicity for depths <15 km (Leon-Rios et al., 2021), and the slab1.0 (Hayes et al., 2012) and slab2.0 (Hayes et al., 2018) models for depths >15 km (Figure 1). To remove possible artifacts in the slab projection, we examine the dependence of the seismic model on the grid node configuration. To do so, we shifted the node positions in the inversion grid by 1/3 of its minimum spacing in the north and east directions and by ±2 km in the vertical component. Each configuration (Table S1 in Supporting Information S1) was first inverted for Vp and then for Vp/Vs. The final models were obtained by averaging the P-wave velocities and Vp/Vs ratios calculated for each grid node setting to ensure robust results. Bootstrapping performed on a subset of the data from our 3DVM showed a standard deviation of 0.3 km/s for Vp and 0.01 for Vp/Vs, while the differences observed between the Vp and Vp/Vs models obtained from the inversions with different node settings are also in this range. To check the model resolution at the slab interface, we performed characteristic recovery tests by evaluating three different sizes of Vp/Vs anomalies (5, 10, and 15 km) distributed along the slab. We focused on the interspersed high (>1.85) and low (<1.82) Vp/Vs features along the slab in the marine forearc (Figure S1 in Supporting Information S1) and calculated synthetic travel time using finite differences to solve the Eikonal equation (Podvin & Lecomte, 1991). Gaussian noise was added based on the weighted variance of the manually picked P-and-S phases (0.05 and 0.1 s, respectively). We then inverted the synthetic arrival time data set first for a minimum 1D model, and then for a 3D velocity model. Finally, we evaluate the differences in the recovered models when both Gaussian noise and station corrections are or are not included in the inversion (Figures S2–S4 in Supporting Information S1). These tests complement the resolution evaluation in Leon-Rios et al. (2021) and show that the recovered models are able to reproduce the synthetic anomalies in both size and amplitude. Adding Gaussian noise and/or station corrections in the inversion does not result in significant differences in the final models.

The Vp model in Figure 1b ranges between 4.5 and 7.2 km/s along the plate interface. We identified a low Vp (~5.5 km/s, L) area, close to the trench at ~0.2°N, which we interpret as either mineralogy changes due to thermal anomalies produced when oceanic crust was formed (Alt, 2004) or shallow serpentinization (Marcaillou et al., 2008). Where the eastern end of the Carnegie Ridge (CR) sits is still under debate; however, our imaged Vp model suggests that the CR terminates close to the coastline. This limit can be linked with the changes in the slab depth observed along the margin, which shows a wider and smoother (i.e., lower angle) dipping region north of the ~0.2°N and a narrower and steeper slab in the southern area (~0.2°N–~0.6°S; Figure 1b). The region between the 10 and 40 km slab-depth contours shows Vp ~ 6.0–7.0 km/s, suggesting a competent region consistent with the typical extent of seismogenic zones (Hyndman et al., 1997; Ruff & Tichelaar, 1996). Below the 40 km slab-depth contour, Vp > 7.2–7.5 km/s is consistent with upper mantle velocities described in this region (e.g., Gailler et al., 2007; Garcia Cano et al., 2014; Figure 1b).

The seismic images also show that, overall, the slab interface is dominated by Vp/Vs of ~1.80–1.84 (Figure 1c), consistent with the average Vp/Vs = 1.82 derived by Leon-Rios et al. (2019). We observe elevated Vp/Vs ratios (>1.84) close to the trench and down to 10 km slab-depth contour, suggesting highly hydrated areas. At the northern end of the CR (~0.0–0.4°N), isolated offshore features with Vp/Vs ~1.80 km/s are associated with seamounts part of the Atacames (At) seamount chain (Marcaillou et al., 2016). Between the 10 and 30 km slab-depth contours, the mixed distribution of low (<1.80) and high (>1.84) Vp/Vs ratios indicates a heterogeneous forearc. At greater depths along the slab interface (>30 km), the Vp/Vs ratios are around 1.82, indicating a less hydrated slab compared to shallow areas close to the trench (Figure 1c).

For the rupture parameters, to the authors' knowledge, the coseismic slip models by Gombert et al. (2018); He et al. (2017); Nocquet et al. (2017); and Yi et al. (2018) are available for the Pedernales earthquake. Here, Gombert et al. (2018) resolved the slip distribution using the most complete data set with near/far field data from inSAR, cGPS, strong motion and tsunami waveforms, obtaining a model with coseismic slip patches up to 8 m (Figure 1). The overlap between the preferred coseismic slip model and our 3DVM shows that the 2016 Pedernales earthquake propagated along a region with Vp ~ 6.5 km/s and Vp/Vs ratios between 1.80 and 1.82. The Vp/Vs range agrees with values for accreted oceanic rocks (Christensen, 1996, 2004; Hyndman et al., 1979). In contrast, at the slab interface where Vp/Vs ratios are elevated (>1.84), aseismic behavior has been proposed to be a prominent feature (Rolandone et al., 2018; Vaca et al., 2018; see Figure 1c). Particularly, the area coinciding with a high Vp/Vs anomaly bounding the SW limit of the Pedernales rupture has been described as a mixed - seismic and aseismic–region (Vallée et al., 2013) showing a coexistence of slow slip processes and seismicity that has occurred repeatedly in the past. These high Vp/Vs anomalies bounding the north-eastern and south-western edges of the distributed coseismic slip and may have contributed to stopping the rupture propagation of the 2016

Pedernales earthquake. In contrast, the areas with Vp/Vs < 1.84 inside the rupture show a positive relationship with the two maxima of the coseismic slip distribution (Figure 1c).

## 4. Quantifying the Relation Between Vp/Vs and Coseismic Slip in Ecuador

We analyzed the distribution of Vp/Vs along the slab interface and compared it with our preferred coseismic slip model, based on the hypothesis that the elevated Vp/Vs ratios (>1.84) could have stopped the rupture propagation. We selected the 2 m coseismic slip contour because it represents the most stable value (closed contour) in the lower range and estimated the rupture area ($A_{2m}$) of 5,660 km$^2$ for the mainshock. To test whether the actual 2016 slip region is particularly favored by moderate Vp/Vs, we examined many other possible earthquake rupture regions. Considering the predominant N-S elongated ruptures observed along the South American subduction zone (Bilek, 2010), we simplified the 2016 rupture to an elliptical shape with a width-length ratio (W/L) of 0.4. This value falls within the W/L range of 0.4–0.7 for $M > 7.0$ earthquakes described in Acharya (1979) for the South American region. Taking the rupture-scaling parameters in Equations 1 and 2 (Allen & Hayes, 2017), we calculated the area of the expected coseismic rupture area ($A_e$) for an Mw 7.8 event, which varies from 7,211 km$^2$ to 7,870 km$^2$, 20%–30% larger than $A_{2m}$.

$$\log(A_{e1}) = a + b\log(\mathrm{Mw});\ a = -3.63, b = 0.63, \mathrm{Mw} = 7.8 \quad (1)$$

$$\log(A_{e2}) = a + b\log(\mathrm{Mw});\ a = -5.62, b = 1.22, \mathrm{Mw} = 7.8 \quad (2)$$

Subsequently, we analyzed three scenarios in which the rupture was shifted by 20 km (scenario 1), 40 km (scenario 2), and 60 km (scenario 3) toward the trench to represent ruptures at different depths (Figure S5 in Supporting Information S1). We have plotted histograms of the Vp/Vs distribution within the coseismic slip for all tested scenarios. We find that the Pedernales earthquake occurred in a region that is mostly covered by Vp/Vs values of 1.80–1.84. The scenarios 1 and 2 show a more dispersed distribution of Vp/Vs ratios, with values ranging from 1.78 to 1.88. Finally, the histogram for scenario 3 shows a region mainly covered by elevated Vp/Vs ratios (~1.86) consistent with the values expected closer to a hydrated and sedimented trench, as in the case of Ecuador. To further extend the possible scenarios, we explore the entire margin affected by the 2016 Pedernales earthquake by following a grid search approach. Here, the simplified rupture area $A_e$ varies in its centroid location every 10 and 15 km in the east-west and north-south directions, respectively (Figure 2). Additionally, we randomly varied the NE striking angle in a range of −10°–30° using a 10°step. The unresolved area >40 km depth was not analyzed.

Based on the overall Vp/Vs ratio of the margin (1.82) and a range of ±~0.02 for regular ratios (e.g., Husen et al., 2000; Nakajima et al., 2001; Reyners et al., 2006, among others), we defined Vp/Vs > 1.84 as high ratios and subsequently mapped their distribution within the ellipse ($A_{vpvs}$) using 1 × 1 km$^2$ histogram bins. We compare the sizes of $A_e$ and $A_{vpvs}$ by introducing a normalized area coefficient, $A_N$ as follows

$$A_N = 1 - A_{vpvs} / A_e \quad (3)$$

Thus, the cases with large $A_N$ illuminate the region most likely to host an Mw 7.8 rupture. We note that the scenarios with maximum values of $A_N$ coincide with the location of the 2016 Pedernales rupture (Figure 2). For the rest of the cases, $A_N$ shows a reduction (Figure S6 in Supporting Information S1) indicating that a large portion of the tested ellipse is covered by elevated Vp/Vs (>1.84), which together with the stress state could contribute to reducing the chances of propagation of a potential earthquake rupture. To evaluate if our results vary depending on the chosen Vp/Vs, we applied the same procedure for Vp/Vs > 1.85 (Figure S7 in Supporting Information S1) and to the characteristic models previously described (Figures S8 and S9 in Supporting Information S1). The results show a similar region for a potential rupture, with the best 20% rupture scenarios having $A_N > 0.97$. These results suggest that the Mw 7.8 Pedernales earthquake occurred in the only area where Vp/Vs is consistently around 1.80–1.84.

## 5. The 1995 Antofagasta, Chile Earthquake

On 30 July 1995, an Mw 8.0 earthquake occurred near Antofagasta city in northern Chile (Delouis et al., 1997; Monfret et al., 1995; Ruegg et al., 1996). Like the Pedernales earthquake, this event is a consequence of the South

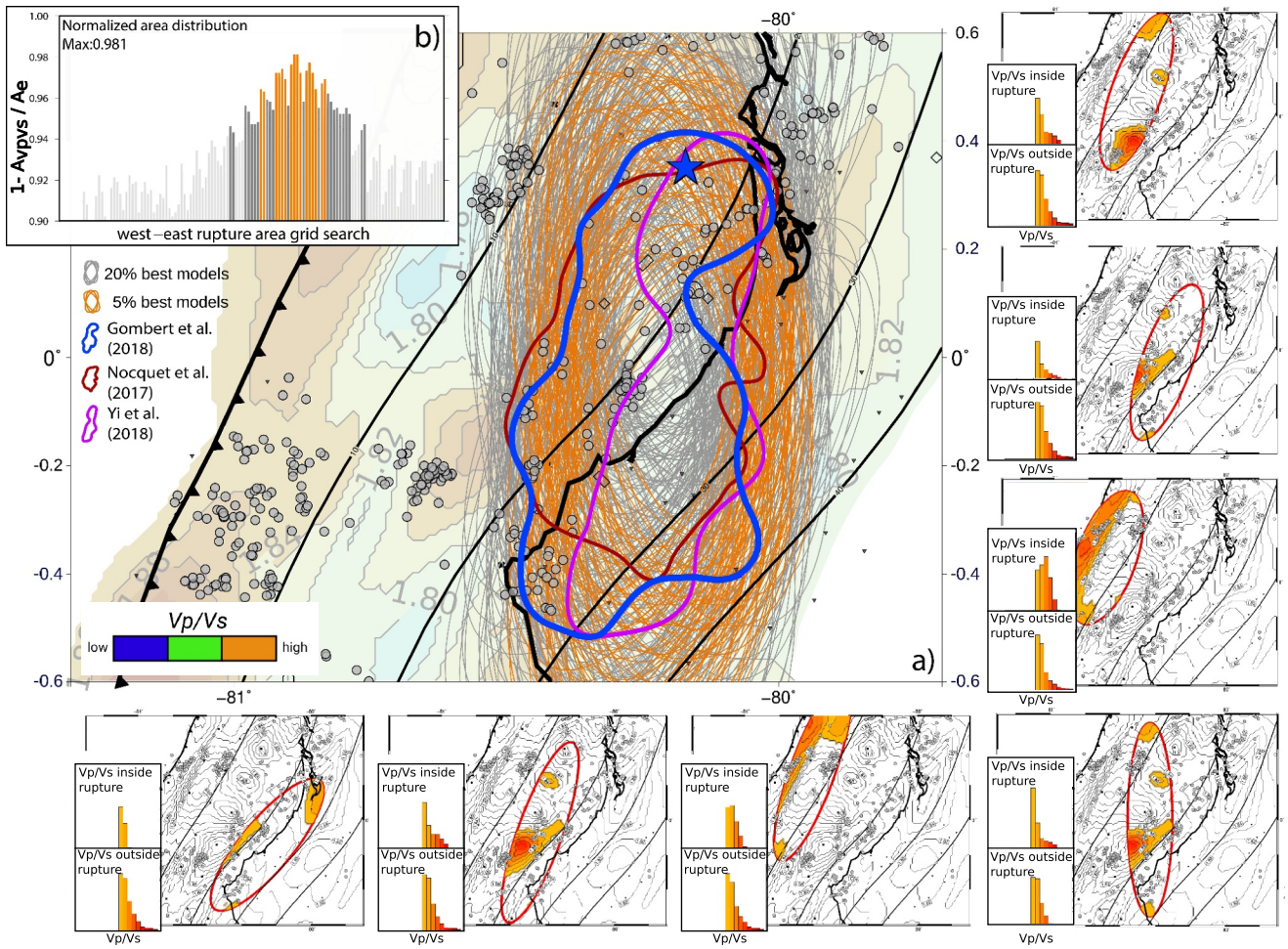


**Figure 2.** (a) Rupture area grid search approach showing the best 20% (gray) and the best 5% (orange) solutions. The 2 m coseismic slip contours from the available slip models are plotted in solid colors. The blue star is the epicenter of the 2016 Pedernales earthquake. The depth slab is contoured every 10 km (black lines). (b) Inset plot shows a stacked histogram of the 1,625 scenarios tested. The 20% and 5% best models use the same color code as in the map view. Inset panels represent a subset of the 1,625 ellipses tested with the grid search. The simplified rupture areas vary in a range of sizes using scaling laws, in striking angles, and in location, covering most of the Ecuadorian margin from the trench to the coast.

American subduction, which in northern Chile has a convergence rate of ∼66–67 mm/yr (Altamimi et al., 2016; Jarrin et al., 2023; Klein et al., 2018; Metois et al., 2016). The Antofagasta earthquake (Figure 3) occurred in a highly segmented region with topographic and bathymetric features, such as the Mejillones Peninsula and the Taltal Ridge (Maksymowicz, 2015) and ruptured a single asperity with a maximum coseismic slip of ∼5–6 m (Chlieh et al., 2004; Pritchard et al., 2002, 2006; Ruegg et al., 1996). In this area, the oceanic plate enters beneath the continental plate with multiple extensional faults from the outer rise (Contreras-Reyes & Carrizo, 2011), promoting fluid circulation along the seismogenic zone (Husen et al., 2000) and heterogeneities along both the upper and downgoing plates (Scholz & Small, 1997). Furthermore, the Taltal ridge, a marine mountain range originating at the San Felix hot spot (Bello-González et al., 2018), contributes with bathymetric features that increase the heterogeneity of the subducting plate between ∼25.0°S and ∼25.5°S. The 1995 Antofagasta earthquake ruptured between 10 and 50 km depth along the megathrust (Delouis et al., 1997). The aftershock distribution shows that most of the events occurred toward the north - limited by the Mejillones Peninsula–and toward the downdip of the rupture (Delouis et al., 1997; Nippress & Rietbrock, 2007). Husen and Kissling (2001) suggested a rapid fluid migration into the overlying plate shortly after the mainshock, which was imaged with high Vp/Vs ratios (>1.79). Afterslip from Pritchard et al. (2006) and aftershocks (M 6–7) during the next 3 years following the mainshock indicate a remanent stress release over time. However, recent geodetic studies from Metois et al. (2016) and Klein et al. (2018) suggest that the area has reached the interseismic stage.

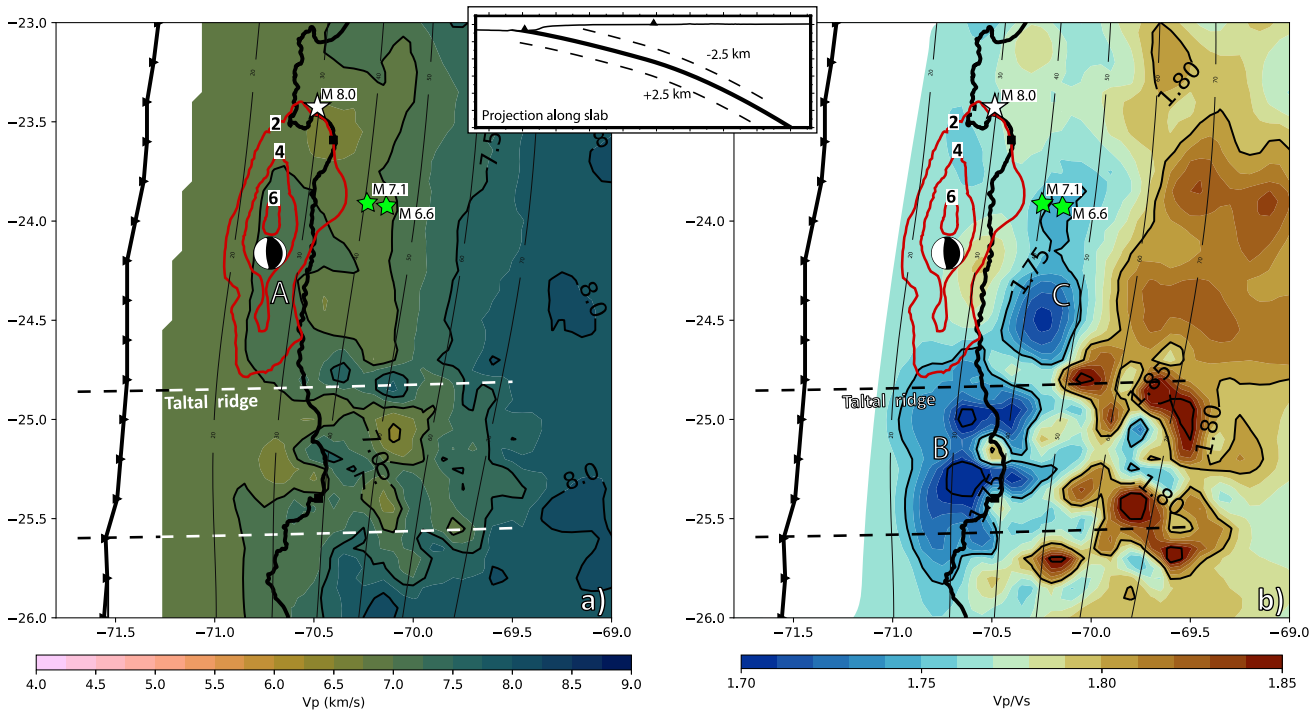


**Figure 3.** (a) Vp and (b) Vp/Vs velocity models projected along a ±2.5 km region around the slab interface (see inset). The stars represent the epicenter of the 1995 Mw 8.0 Antofagasta earthquake (white) and the two largest aftershocks (green). The solid red line shows the corresponding coseismic slip contour by Pritchard et al. (2006), which is limited by the Mejillones Peninsula to the north and the Taltal ridge to the south. The seismic velocity models were determined by a regional experiment that used 84 stations and collected data during 8 months, from March to October 2020 (Leon-Rios et al., 2024).

We tested the relationship between physical properties along the slab interface and the distribution of coseismic slip using the same approach as described for the Pedernales earthquake. For this, we used the 3DVM by Leon-Rios et al. (2024) and the slip model from Pritchard et al. (2002, 2006). The velocity model for the area was obtained with 84 stations that recorded over a period of 8 months in 2020. Without offshore instrumentation, our resolution - recovered after standard checkerboard tests of 10, 15 and 20 km synthetic anomalies of ±5% of the original velocity (Figure S10 in Supporting Information S1)–only allows us to discuss the central and downdip extent of the Antofagasta rupture. We observe that the area where the Antofagasta earthquake had the maximum coseismic slip is aligned with an N-S elongated Vp ~7 km/s anomaly (A in Figure 3). As expected, this observation suggests that the rupture is more likely to propagate in a rapid—therefore stronger—medium. For the Vp/Vs model (Figure 3), we find a strong correlation between the Vp/Vs anomalies and the limits of the rupture although opposite to the observed for Ecuador. When comparing seismic velocity sections by Husen and Kissling (2001) and Leon-Rios et al. (2024), we observe similarities in the Vp/Vs distribution, especially with the early-stage image shortly after the mainshock. Although the models were determined at different times along the seismic cycle, this observation contributes to identifying persistent features both at the coseismic-early post-seismic (Husen & Kissling, 2001) and the interseismic (Leon-Rios et al., 2024). Now, by contrasting our 3DVM with the slip distribution, we observe that to the north, the 2–4 m coseismic slip distribution is bound by a low (<1.75) anomaly located close to the Mejillones Peninsula, which has been described as a barrier for large earthquakes (Bilek, 2010; Maksymowicz, 2015; Watts et al., 2010). To the south, the 2 m coseismic slip contour is controlled by a large anomaly with low Vp/Vs (<1.75, B in Figure 3). This feature is well aligned with the swell of the Taltal ridge and is consistent with observations that identify these types of topographic highs as barriers for earthquake rupture extent (Contreras-Reyes & Carrizo, 2011). Furthermore, we observe how the trajectory of the Taltal ridge is consistent with a more heterogeneous onshore region in both the Vp and Vp/Vs models, and also has implications in the overriding plate with evidence of erosive processes in the coastal scarp and over the coastline (Figure 3). Finally, at depths between 40 and 50 km, a ~70 km N-S oriented low (1.75) Vp/Vs anomaly (C in Figure 3) controls the downdip of the coseismic slip. Here, we also find a positive relationship between the bounds of this anomaly and the aftershock seismicity reported in the following 3.3 years after the 1995 mainshock

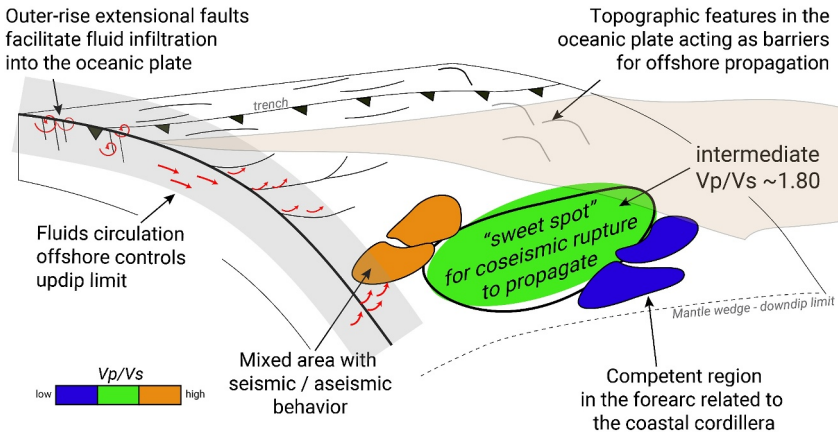


**Figure 4.** Summary sketch. Trenchward, bending faults and subducting topography promote fluid circulation and infiltration into the oceanic plate. Offshore, fluid circulation influences the updip limit of ruptures. Along the seismogenic zone, high Vp/Vs (>1.84) anomalies correspond to regions of mixed seismic and aseismic behavior, potentially controlling the extent of moderate earthquakes. In contrast, low Vp/Vs (<1.75) are related to competent regions, such as coastal cordillera, and appear to control the downdip rupture limit. For the two cases studied in this work, earthquake ruptures propagate within a "sweet spot" characterized by intermediate Vp/Vs (~1.80), where optimal fluid content and porosity facilitate rupture propagation. These seismic anomalies highlight key physical properties that may play a critical role in controlling the size and hence magnitude of earthquakes.

event (Chlieh et al., 2004). This feature is a large structure part of the coastal batholith (Pichowiak, 1994; Taylor et al., 1998), that extends from the surface down to the slab interface, and which has also been observed in previous seismic tomography images (Husen et al., 2000) and other geophysical methods such as magneto-tellurics (Slezak et al., 2021). Therefore, the downdip limit of the Antofagasta earthquake appears to be controlled by a large upper plate structure that extends down to the slab interface. Moreover, the stress adjustment over time after the mainshock also seems to be controlled by this feature, which has hosted the largest aftershocks of the sequence (M6.6 and M7.1, Figure 3).

## 6. Conclusion

The integration of seismic tomography, slip distribution, rupture scaling relations, and a grid search approach allowed the characterization of seismic anomalies that influence slip behavior along the plate interface. Analysis of two case studies shows that earthquake rupture zones seems to predominantly propagate through regions of intermediate Vp/Vs (~1.80), while rupture boundaries were associated with higher (>1.84 for Ecuador) or lower (<1.75 for northern Chile) Vp/Vs anomalies (Figure 4). These heterogeneities likely constrained coseismic slip propagation of the two study cases. We observe that regions with intermediate Vp/Vs values appear to function as a mechanical "sweet spot" where the interaction of fluid distribution, porosity, effective stress, and elastic properties optimizes conditions for sustained rupture propagation. In contrast, pronounced deviations from this optimal region, delineated by higher or lower Vp/Vs anomalies, likely serve as structural and rheological barriers that limit rupture extent and control the maximum magnitude of megathrust earthquakes (Figure 4). Whether the link between seismic velocities and coseismic slip is observed in larger earthquakes (M8.5+), the velocity structure derived after the 2010 Mw 8.8 Maule, Chile earthquake (Hicks et al., 2014; Moreno et al., 2014) or the 2011 Mw 9.0 Tohoku-Oki earthquake (Yamamoto et al., 2014) shows that the largest amplitudes of coseismic slip spread along the margin without discriminating specific changes in seismic velocities. In both cases, changes in the velocity structure may not be sufficient to control the rupture limits due to the large magnitude of the events (>8.5) and thus the amount of energy released. Although further analysis of other megathrust earthquakes and better offshore constraints of seismic velocity models are needed, our observations along the South American margin can shed light on the capacities of combining both seismic velocity and coseismic slip models for revealing rupture-prone areas and the likely magnitude of potential earthquakes, providing relevant information for seismic hazard assessment.

## Data Availability Statement

For the Ecuador deployment, raw data, velocity models, earthquake catalog and software used are located at IRIS website http://www.iris.edu/dms/nodes/dmc/ using the network code 8G (Meltzer & Beck, 2016), G (Institut de Physique du Globe de Paris & Ecole et Observatoire des Sciences de la Terre de Strasbourg, 1982) and EC (Instituto Geofisico). Data from the emergency deployment XE is available through Regnier et al. (2016). The Earthquakes catalog is available through Agurto-Detzel et al. (2019). Model data are available in the KIT open repository (Leon-Rios & Rietbrock, 2020). Temporary X5-Taltal network details in the FDSN database (Rietbrock et al., 2020). Raw data will be available on the FDSN/EIDA server hosted by GFZ-Potsdam (Rietbrock, 2024). Initial and final models as well as hypocenter catalog, arrival times, and processing algorithms user guides are available in ZENODO (Leon-Rios, 2023).

**Acknowledgments**
This work supported in part by NSF-China-ANID PI18003, ANID under Project AFB180004 and ANID/BASAL AFB230001, IGEPN, IRD, INSU-CNRS, and ANR-15-CE04-0004. The UK deployment was supported by NERC NE/P008828/1. The US deployment was supported by IRIS PASSCAL and NSF RAPID Program EAR-1642498. SLR acknowledges partial support from ANID BecasChile (Grant 8068/2015) and ANID Fondecyt Postdoctorado 2022(3220039). Open Access funding enabled and organized by Projekt DEAL.

## References

Acharya, H. K. (1979). A method to determine the duration of quiescence in a seismic gap. *Geophysical Research Letters*, *6*(9), 681–684. https://doi.org/10.1029/gl006i009p00681

Agurto-Detzel, H., Font, Y., Charvis, P., Régnier, M., Rietbrock, A., Ambrois, D., et al. (2019). Ridge subduction and after slip control aftershock distribution of the 2016 Mw 7.8 Ecuador earthquake. *Earth and Planetary Science Letters*, *520*, 63–76. https://doi.org/10.1016/j.epsl.2019.05.029

Allen, T. I., & Hayes, G. P. (2017). Alternative rupture-scaling relationships for subduction interface and other offshore environments. *Bulletin of the Seismological Society of America*, *107*(3), 1240–1253. https://doi.org/10.1785/0120160255

Alt, J. C. (2004). Alteration of the upper oceanic crust: Mineralogy, chemistry, and processes. *Hydrogeology of the oceanic lithosphere*, *1*, 495–533.

Altamimi, Z., Rebischung, P., Métivier, L., & Collilieux, X. (2016). ITRF2014: A new release of the international terrestrial reference frame modeling nonlinear station motions. *Journal of Geophysical Research: Solid Earth*, *121*(8), 6109–6131. https://doi.org/10.1002/2016jb013098

Audet, P., & Schwartz, S. Y. (2013). Hydrologic control of fore arc strength and seismicity in the Costa Rican subduction zone. *Nature Geoscience*, *6*(10), 852–855. https://doi.org/10.1038/ngeo1927

Bello-González, J. P., Contreras-Reyes, E., & Arriagada, C. (2018). Predicted path for hotspot tracks off South America since Paleocene times: Tectonic implications of ridge-trench collision along the Andean margin. *Gondwana Research*, *64*, 216–234. https://doi.org/10.1016/j.gr.2018.07.008

Bilek, S. L. (2010). Invited review paper: Seismicity along the South American subduction zone: Review of large earthquakes, tsunamis, and subduction zone complexity. *Tectonophysics*, *495*(1–2), 2–14. https://doi.org/10.1016/j.tecto.2009.02.037

Bilek, S. L., Schwartz, S. Y., & DeShon, H. R. (2003). Control of seafloor roughness on earthquake rupture behavior. *Geology*, *31*(5), 455–458. https://doi.org/10.1130/0091-7613(2003)031<0455:cosroe>2.0.co;2

Byrne, D. E., Davis, D. M., & Sykes, L. R. (1988). Loci and maximum size of thrust earthquakes and the mechanics of the shallow region of subduction zones. *Tectonics*, *7*(4), 833–857. https://doi.org/10.1029/tc007i004p00833

Chalumeau, C., Agurto-Detzel, H., De Barros, L., Charvis, P., Galve, A., Rietbrock, A., et al. (2021). Repeating earthquakes at the edge of the after slip of the 2016 Ecuadorian MW7.8 Pedernales earthquake. *Journal of Geophysical Research: Solid Earth*, *126*(5), e2021JB021746. https://doi.org/10.1029/2021jb021746

Chalumeau, C., Agurto-Detzel, H., Rietbrock, A., Frietsch, M., Oncken, O., Segovia, M., & Galve, A. (2024). Seismological evidence for a multifault network at the subduction interface. *Nature*, *628*(8008), 558–562. https://doi.org/10.1038/s41586-024-07245-y

Chlieh, M., De Chabalier, J. B., Ruegg, J. C., Armijo, R., Dmowska, R., Campos, J., & Feigl, K. L. (2004). Crustal deformation and fault slip during the seismic cycle in the north Chile subduction zone, from GPS and InSAR observations. *Geophysical Journal International*, *158*(2), 695–711. https://doi.org/10.1111/j.1365-246x.2004.02326.x

Christensen, N. I. (1996). Poisson's ratio and crustal seismology. *Journal of Geophysical Research*, *101*(B2), 3139–3156. https://doi.org/10.1029/95jb03446

Christensen, N. I. (2004). Serpentinites, peridotites, and seismology. *International Geology Review*, *46*(9), 795–816. https://doi.org/10.2747/0020-6814.46.9.795

Collot, J. Y., Migeon, S., Spence, G., Legonidec, Y., Marcaillou, B., Schneider, J. L., et al. (2005). Seafloor margin map helps in understanding subduction earthquakes. *Eos, Transactions American Geophysical Union*, *86*(46), 463–465. https://doi.org/10.1029/2005eo460003

Collot, J. Y., Sanclemente, E., Nocquet, J. M., Leprêtre, A., Ribodetti, A., Jarrin, P., et al. (2017). Subducted Oceanic relief locks the shallow megathrust in central Ecuador. *Journal of Geophysical Research: Solid Earth*, *122*(5), 3286–3305. https://doi.org/10.1002/2016jb013849

Contreras-Reyes, E., & Carrizo, D. (2011). Control of high oceanic features and subduction channel on earthquake ruptures along the Chile–Peru subduction zone. *Physics of the Earth and Planetary Interiors*, *186*(1–2), 49–58. https://doi.org/10.1016/j.pepi.2011.03.002

Delouis, B., Monfret, T., Dorbath, L., Pardo, M., Rivera, L., Comte, D., et al. (1997). The Mw=8.0 Antofagasta (northern Chile) earthquake of 30 July 1995: A precursor to the end of the large 1877 gap. *Bulletin of the Seismological Society of America*, *87*(2), 427–445. https://doi.org/10.1785/bssa0870020427

Di Stefano, R., Chiarabba, C., Chiaraluce, L., Cocco, M., De Gori, P., Piccinini, D., & Valoroso, L. (2011). Fault zone properties affecting the rupture evolution of the 2009 ($M_w$ 6.1) L'Aquila earthquake (central Italy): Insights from seismic tomography. *Geophysical Research Letters*, *38*(10), L10310. https://doi.org/10.1029/2011GL047365

Gailler, A., Charvis, P., & Flueh, E. R. (2007). Segmentation of the Nazca and South American plates along the Ecuador subduction zone from wide angle seismic profiles. *Earth and Planetary Science Letters*, *260*(3–4), 444–464. https://doi.org/10.1016/j.epsl.2007.05.045

Galve, A. (2020). HIPER cruise, RV L'Atalante. https://doi.org/10.17600/18001348

Galve, A., Rietbrock, A., Charvis, P., De la Torre, G., Vaca, S., Segovia, M., et al. (2021). How fluids impact seismic/aseismic slip in the Ecuadorian subduction zone? The hiper marine project. In *EGU general assembly conference abstracts* (pp. EGU21–EGU10988).

Garcia Cano, L. C., Galve, A., Charvis, P., & Marcaillou, B. (2014). Three-dimensional velocity structure of the outer fore arc of the Colombia-Ecuador subduction zone and implications for the 1958 megathrust earthquake rupture zone. *Journal of Geophysical Research: Solid Earth*, *119*(2), 1041–1060. https://doi.org/10.1002/2012jb009978

Gombert, B., Duputel, Z., Jolivet, R., Simons, M., Jiang, J., Liang, C., et al. (2018). Strain budget of the Ecuador–Colombia subduction zone: A stochastic view. *Earth and Planetary Science Letters*, *498*, 288–299. https://doi.org/10.1016/j.epsl.2018.06.046

Haberland, C., Rietbrock, A., Lange, D., Bataille, K., & Dahm, T. (2009). Structure of the seismogenic zone of the south central Chilean margin revealed by local earthquake travel time tomography. *Journal of Geophysical Research*, *114*(B1), B01317. https://doi.org/10.1029/2008jb005802

Hayes, G. P., Moore, G. L., Portner, D. E., Hearne, M., Flamme, H., Furtney, M., & Smoczyk, G. M. (2018). Slab2, a comprehensive subduction zone geometry model. *Science*, *362*(6410), 58–61. https://doi.org/10.1126/science.aat4723

Hayes, G. P., Wald, D. J., & Johnson, R. L. (2012). Slab1. 0: A three-dimensional model of global subduction zone geometries. *Journal of Geophysical Research*, *117*(B1), B01302. https://doi.org/10.1029/2011jb008524

He, P., Hetland, E. A., Wang, Q., Ding, K., Wen, Y., & Zou, R. (2017). Coseismic slip in the 2016 Mw 7.8 Ecuador earthquake imaged from Sentinel-1A radar interferometry. *Seismological Research Letters*, *88*(2A), 277–286. https://doi.org/10.1785/0220160151

Hicks, S. P., Rietbrock, A., Ryder, I. M., Lee, C. S., & Miller, M. (2014). Anatomy of a megathrust: The 2010 M8. 8 Maule, Chile earthquake rupture zone imaged using seismic tomography. *Earth and Planetary Science Letters*, *405*, 142–155.

Husen, S., & Kissling, E. (2001). Postseismic fluid flow after the large subduction earthquake of Antofagasta, Chile. *Geology*, *29*(9), 847–850. https://doi.org/10.1130/0091-7613(2001)029<0847:pffatl>2.0.co;2

Husen, S., Kissling, E., & Flueh, E. R. (2000). Local earthquake tomography of shallow subduction in north Chile: A combined onshore and offshore study. *Journal of Geophysical Research*, *105*(B12), 28183–28198. https://doi.org/10.1029/2000jb900229

Hyndman, R. D., Christensen, N. I., & Drury, M. J. (1979). Seismic velocities, densities, electrical resistivities, porosities and thermal conductivities of core samples from boreholes into the islands of Bermuda and the Azores. *Deep Drilling Results in the Atlantic Ocean: Ocean Crust*, *2*, 94–112. https://doi.org/10.1029/me002p0094

Hyndman, R. D., & Wang, K. (1993). Thermal constraints on the zone of major thrust earthquake failure: The Cascadia subduction zone. *Journal of Geophysical Research*, *98*(B2), 2039–2060. https://doi.org/10.1029/92jb02279

Hyndman, R. D., Yamano, M., & Oleskevich, D. A. (1997). The seismogenic zone of subduction thrust faults. *Island Arc*, *6*(3), 244–260. https://doi.org/10.1111/j.1440-1738.1997.tb00175.x

Institut de physique du globe de Paris (IPGP), & École et Observatoire des Sciences de la Terre de Strasbourg (EOST). (1982). *GEOSCOPE, French Global Network of broad band seismic stations*. Institut de physique du globe de Paris (IPGP), Université de Paris. https://doi.org/10.18715/GEOSCOPE.G

Jarrin, P., Nocquet, J. M., Rolandone, F., Audin, L., Mora-Páez, H., Alvarado, A., et al. (2023). Continental block motion in the Northern Andes from GPS measurements. *Geophysical Journal International*, *235*(2), 1434–1464. https://doi.org/10.1093/gji/ggad294

Klein, E., Metois, M., Meneses, G., Vigny, C., & Delorme, A. (2018). Bridging the gap between North and Central Chile: Insight from new GPS data on coupling complexities and the Andean sliver motion. *Geophysical Journal International*, *213*(3), 1924–1933. https://doi.org/10.1093/gji/ggy094

Leon-Rios, S. (2023). Research data for Taltal segment tomography article [Dataset]. *Zenodo*. https://doi.org/10.5281/zenodo.8271327

Leon-Rios, S., Agurto-Detzel, H., Rietbrock, A., Alvarado, A., Beck, S., Charvis, P., et al. (2019). 1D-velocity structure and seismotectonics of the Ecuadorian margin inferred from the 2016 Mw7.8 Pedernales aftershock sequence. *Tectonophysics*, *767*, 228165. https://doi.org/10.1016/j.tecto.2019.228165

Leon-Rios, S., Bie, L., Agurto-Detzel, H., Rietbrock, A., Galve, A., Alvarado, A., et al. (2021). 3D local earthquake tomography of the Ecuadorian margin in the source area of the 2016 Mw 7.8 Pedernales earthquake. *Journal of Geophysical Research: Solid Earth*, *126*(3), e2020JB020701. https://doi.org/10.1029/2020jb020701

Leon-Rios, S., Reyes-Wagner, V., Calle-Gardella, D., Rietbrock, A., Roecker, S., Maksymowicz, A., & Comte, D. (2024). Structural characterization of the taltal segment in Northern Chile between 22°S and 26°S using local earthquake tomography. *Geochemistry, Geophysics, Geosystems*, *25*(5), e2023GC011197. https://doi.org/10.1029/2023gc011197

Leon-Rios, S., & Rietbrock, A. (2020). Research data for "3D local earthquake tomography of the Ecuadorian margin in the source area of the 2016 Mw 7.8 Pedernales earthquake". https://doi.org/10.5445/IR/1000126350

Liu, C., An, C., Shan, B., Xiong, X., & Chen, X. (2018). Insights into the kinematic rupture of the 2015 Mw 8.3 Illapel, Chile, earthquake from joint analysis of geodetic, seismological, tsunami, and superconductive gravimeter observations. *Journal of Geophysical Research: Solid Earth*, *123*(11), 9778–9799. https://doi.org/10.1029/2018jb016065

Maksymowicz, A. (2015). The geometry of the Chilean continental wedge: Tectonic segmentation of subduction processes off Chile. *Tectonophysics*, *659*, 183–196. https://doi.org/10.1016/j.tecto.2015.08.007

Marcaillou, B., Collot, J. Y., Ribodetti, A., d'Acremont, E., Mahamat, A. A., & Alvarado, A. (2016). Seamount subduction at the North-Ecuadorian convergent margin: Effects on structures, inter-seismic coupling and seismogenesis. *Earth and Planetary Science Letters*, *433*, 146–158. https://doi.org/10.1016/j.epsl.2015.10.043

Marcaillou, B., Spence, G., Wang, K., Collot, J. Y., & Ribodetti, A. (2008). Thermal segmentation along the N. Ecuador–S. Colombia margin (1–4 N): Prominent influence of sedimentation rate in the trench. *Earth and Planetary Science Letters*, *272*(1–2), 296–308. https://doi.org/10.1016/j.epsl.2008.04.049

Meltzer, A., & Beck, S. (2016). 2016 Pedernales earthquake aftershock deployment Ecuador [Dataset]. *International Federation of Digital Seismograph Networks*. https://doi.org/10.7914/SN/8G_2016

Meltzer, A., Beck, S., Ruiz, M., Hoskins, M., Soto-Cordero, L., Stachnik, J. C., et al. (2019). The 2016 Mw 7.8 Pedernales, Ecuador, earthquake: Rapid response deployment. *Seismological Research Letters*, *90*(3), 1346–1354. https://doi.org/10.1785/0220180364

Metois, M., Vigny, C., & Socquet, A. (2016). Interseismic coupling, megathrust earthquakes and seismic swarms along the Chilean subduction zone (38–18 S). *Pure and Applied Geophysics*, *173*(5), 1431–1449. https://doi.org/10.1007/s00024-016-1280-5

Miller, P. K., Saffer, D. M., Abers, G. A., Shillington, D. J., Bécel, A., Li, J., & Bate, C. (2021). P- and S-wave velocities of exhumed metasediments from the Alaskan subduction zone: Implications for the in situ conditions along the megathrust. *Geophysical Research Letters*, *48*(20), e2021GL094511. https://doi.org/10.1029/2021gl094511

Mishra, O. P., Zhao, D., Umino, N., & Hasegawa, A. (2003). Tomography of northeast Japan forearc and its implications for interplate seismic coupling. *Geophysical Research Letters*, *30*(16), 1850. https://doi.org/10.1029/2003gl017736

Monfret, T., Dorbath, L., Caminade, J. P., Pardo, M., Comte, D., & Ponce, L. (1995). The July 30, Antofagasta earthquake: An hypocritical seismic event. *Eos, Transactions, American Geophysical Union*, *76*, 427.

Moreno, M., Haberland, C., Oncken, O., Rietbrock, A., Angiboust, S., & Heidbach, O. (2014). Locking of the Chile subduction zone controlled by fluid pressure before the 2010 earthquake. *Nature Geoscience*, *7*(4), 292–296. https://doi.org/10.1038/ngeo2102

Nakajima, J., Matsuzawa, T., Hasegawa, A., & Zhao, D. (2001). Three-dimensional structure of Vp, Vs, and Vp/Vs beneath northeastern Japan: Implications for arc magmatism and fluids. *Journal of Geophysical Research*, *106*(B10), 21843–21857.

Nippress, S. E. J., & Rietbrock, A. (2007). Seismogenic zone high permeability in the central Andes inferred from relocations of micro-earthquakes. *Earth and Planetary Science Letters*, *263*(3–4), 235–245. https://doi.org/10.1016/j.epsl.2007.08.032

Nocquet, J. M., Jarrin, P., Vallée, M., Mothes, P. A., Grandin, R., Rolandone, F., et al. (2017). Supercycle at the Ecuadorian subduction zone revealed after the 2016 Pedernales earthquake. *Nature Geoscience*, *10*(2), 145–149. https://doi.org/10.1038/ngeo2864

Nocquet, J. M., Villegas-Lanza, J. C., Chlieh, M., Mothes, P. A., Rolandone, F., Jarrin, P., et al. (2014). Motion of continental slivers and creeping subduction in the northern Andes. *Nature Geoscience*, *7*(4), 287–291. https://doi.org/10.1038/ngeo2099

Pasten-Araya, F., Salazar, P., Ruiz, S., Rivera, E., Potin, B., Maksymowicz, A., et al. (2018). Fluids along the plate interface influencing the frictional regime of the Chilean subduction zone, northern Chile. *Geophysical Research Letters*, *45*(19), 10–378. https://doi.org/10.1029/2018gl079283

Pichowiak, S. (1994). Early Jurassic to early Cretaceous magmatism in the coastal cordillera and the central depression of north Chile. In *Tectonics of the southern central andes: Structure and evolution of an active continental margin* (pp. 203–217). Springer Berlin Heidelberg.

Podvin, P., & Lecomte, I. (1991). Finite difference computation of travel times in very contrasted velocity models: A massively parallel approach and its associated tools. *Geophysical Journal International*, *105*(1), 271–284. https://doi.org/10.1111/j.1365-246x.1991.tb03461.x

Pritchard, M. E., Ji, C., & Simons, M. (2006). Distribution of slip from 11 Mw>6 earthquakes in the northern Chile subduction zone. *Journal of Geophysical Research*, *111*(B10), B10302. https://doi.org/10.1029/2005jb004013

Pritchard, M. E., Simons, M., Rosen, P. A., Hensley, S., & Webb, F. H. (2002). Co-seismic slip from the 1995 July 30 Mw=8.1 Antofagasta, Chile, earthquake as constrained by InSAR and GPS observations. *Geophysical Journal International*, *150*(2), 362–376. https://doi.org/10.1046/j.1365-246x.2002.01661.x

Regnier, M., Font, Y., Charvis, P., Mercerat, D., Rietbrock, A., Ruiz, M., & Alvarado, A. (2016). Pedernales [Dataset]. *International Federation of Digital Seismograph Networks*. https://doi.org/10.7914/SN/XE_2016

Reyners, M., & Eberhart-Phillips, D. (2009). Small earthquakes provide insight into plate coupling and fluid distribution in the Hikurangi subduction zone, New Zealand. *Earth and Planetary Science Letters*, *282*(1–4), 299–305. https://doi.org/10.1016/j.epsl.2009.03.034

Reyners, M., Eberhart-Phillips, D., Stuart, G., & Nishimura, Y. (2006). Imaging subduction from the trench to 300 km depth beneath the central North Island, New Zealand, with Vp and Vp/Vs. *Geophysical Journal International*, *165*(2), 565–583. https://doi.org/10.1111/j.1365-246x.2006.02897.x

Rietbrock, A. (2024). *Taltal seismological network*. Karlsruhe Institute of Technology. https://doi.org/10.35097/dIDjKJPeUpZFWjbQ

Rietbrock, A., Comte, D., & Leon-Rios, S. (2020). Taltal temporary deployment [Dataset]. *International Federation of Digital Seismograph Networks*. https://doi.org/10.7914/mc8r-ft72

Rolandone, F., Nocquet, J. M., Mothes, P. A., Jarrin, P., Vallée, M., Cubas, N., et al. (2018). Areas prone to slow slip events impede earthquake rupture propagation and promote after slip. *Science Advances*, *4*(1), eaao6596. https://doi.org/10.1126/sciadv.aao6596

Ruegg, J. C., Campos, J., Armijo, R., Barrientos, S., Briole, P., Thiele, R., et al. (1996). The Mw=8.1 Antofagasta (North Chile) earthquake of July 30, 1995: First results from teleseismic and geodetic data. *Geophysical Research Letters*, *23*(9), 917–920. https://doi.org/10.1029/96gl01026

Ruff, L. J., & Tichelaar, B. W. (1996). What controls the seismogenic plate interface in subduction zones? *Geophysical Monograph Series*, *96*, 105–111. https://doi.org/10.1029/gm096p0105

Scholz, C. H., & Small, C. (1997). The effect of seamount subduction on seismic coupling. *Geology*, *25*(6), 487–490. https://doi.org/10.1130/0091-7613(1997)025<0487:teosso>2.3.co;2

Segovia, M. (2009). *Análisis espacio-temporal del Enjambre de Puerto López entre enero y febrero de 2005 con observaciones de la estación de banda ancha de OTAVALO, Master Thesis*. University of Nice Sophia Antipolis. (in Spanish).

Segovia, M., Font, Y., Régnier, M., Charvis, P., Galve, A., Nocquet, J. M., et al. (2018). Seismicity distribution near a subducting seamount in the Central Ecuadorian subduction zone, space-time relation to a slow-slip event. *Tectonics*, *37*(7), 2106–2123. https://doi.org/10.1029/2017tc004771

Slezak, K., Díaz, D., Vargas, J. A., Cordell, D., Reyes-Cordova, F., & Segovia, M. J. (2021). Magnetotelluric image of the Chilean subduction zone in the Salar de Atacama region (23°–24° S): Insights into factors controlling the distribution of volcanic arc magmatism. *Physics of the Earth and Planetary Interiors*, *318*, 106765. https://doi.org/10.1016/j.pepi.2021.106765

Sobiesiak, M. M., Meyer, U., Schmidt, S., Götze, H. J., & Krawczyk, C. (2007). Asperity generating upper crustal sources revealed by b-value and isostatic residual anomaly grids in the area of Antofagasta. *Journal of Geophysical Research*, *112*(B12), B12308. https://doi.org/10.1029/2006jb004796

Soto-Cordero, L., Meltzer, A., Bergman, E., Hoskins, M., Stachnik, J. C., Agurto-Detzel, H., et al. (2020). Structural control on megathrust rupture and slip behavior: Insights from the 2016 Mw 7.8 Pedernales Ecuador earthquake. *Journal of Geophysical Research: Solid Earth*, *125*(2), e2019JB018001. https://doi.org/10.1029/2019jb018001

Taylor, G. K., Grocott, J., Pope, A., & Randall, D. E. (1998). Mesozoic fault systems, deformation and fault block rotation in the Andean forearc: A crustal scale strike-slip duplex in the coastal Cordillera of northern Chile. *Tectonophysics*, *299*(1–3), 93–109. https://doi.org/10.1016/s0040-1951(98)00200-5

Tichelaar, B. W., & Ruff, L. J. (1993). Depth of seismic coupling along subduction zones. *Journal of Geophysical Research*, *98*(B2), 2017–2037. https://doi.org/10.1029/92jb02045

Vaca, S., Régnier, M., Bethoux, N., Alvarez, V., & Pontoise, B. (2009). Sismicidad de la región de Manta: Enjambre sísmico de Manta-2005. In J.-Y. Collot, V. Sallarès, & A. Pazmiño (Eds.), *Geología y Geofísica Marina y Terrestre del Ecuador desde la costa continental hasta las Islas Galápagos, PSE-001-2009* (pp. 155–166). Guayaquil: Comisión Nacional del Derecho del Mar (CNDM). (in Spanish).

Vaca, S., Vallée, M., Nocquet, J. M., Battaglia, J., & Régnier, M. (2018). Recurrent slow slip events as a barrier to the northward rupture propagation of the 2016 Pedernales earthquake (central Ecuador). *Tectonophysics*, *724*, 80–92.

Vallée, M., Nocquet, J. M., Battaglia, J., Font, Y., Segovia, M., Régnier, M., et al. (2013). Intense interface seismicity triggered by a shallow slow slip event in the central Ecuador subduction zone. *Journal of Geophysical Research: Solid Earth*, *118*(6), 2965–2981. https://doi.org/10.1002/jgrb.50216

Vrolijk, P. (1990). On the mechanical role of smectite in subduction zones. *Geology*, *18*(8), 703–707. https://doi.org/10.1130/0091-7613(1990)018<0703:otmros>2.3.co;2

Wang, K., & Bilek, S. L. (2011). Do subducting seamounts generate or stop large earthquakes? *Geology*, *39*(9), 819–822. https://doi.org/10.1130/g31856.1

Watts, A. B., Koppers, A. A., & Robinson, D. P. (2010). Seamount subduction and earthquakes. *Oceanography*, *23*(1), 166–173. https://doi.org/10.5670/oceanog.2010.68

Wiemer, S., & Katsumata, K. (1999). Spatial variability of seismicity parameters in aftershock zones. *Journal of Geophysical Research*, *104*(B6), 13135–13151. https://doi.org/10.1029/1999JB900032

Yamamoto, Y., Obana, K., Kodaira, S., Hino, R., & Shinohara, M. (2014). Structural heterogeneities around the megathrust zone of the 2011 Tohoku earthquake from tomographic inversion of onshore and offshore seismic observations. *Journal of Geophysical Research: Solid Earth*, *119*(2), 1165–1180. https://doi.org/10.1002/2013jb010582

Yi, L., Xu, C., Wen, Y., Zhang, X., & Jiang, G. (2018). Rupture process of the 2016 Mw 7.8 Ecuador earthquake from joint inversion of InSAR data and teleseismic P waveforms. *Tectonophysics*, *722*, 163–174. https://doi.org/10.1016/j.tecto.2017.10.028